Materials Science-Poland, Vol. 23, No. 2, 2005

Coupled space-time multiscale simulations of dynamic delamination tests

STEFANO MARIANI [1*], ANNA PANDOLFI[1], RAFFAELLA PAVANI[2]

[1]Dipartimento di Ingegneria Strutturale, Politecnico di Milano,
Piazza L. da Vinci 32, 20133 – Milano, Italy

[2]Dipartimento di Matematica "Francesco Brioschi", Politecnico di Milano,
Piazza L. da Vinci 32, 20133 – Milano, Italy

The aim of this work was to numerically investigate the dynamic debonding of a thin composite laminate from a rigid substrate. The laminate is elastic and the separation surface behaviour is governed by a cohesive softening law. By way of simplification, the bending dominated deflection of the free part of the laminate is described through the Euler–Bernoulli kinematics. In this context, the partial differential equation governing the laminate motion is characterized by two length scales and two time scales. To accurately simulate the growth of delamination, a coupled space-time multiscale integration was used. The qualifying features of such an approach are: i) a fine spatial discretization across the process zone, where the evolution of the cohesive tractions demands a detailed description; ii) a high order accurate time integration algorithm, capable of damping spurious high frequency oscillations of the solution. The results of a two-stage peel test testify to the good performance of the approach applied.

Key words: *non-linear dynamic fracture mechanics*; *delamination*; *heterogeneous multiscale method*

1. Introduction

The failure of composite structures under dynamic loading is in need of deep investigation, as the recently published literature testifies (see, e.g., [1–6]). The research has two main objectives: i) the development of ad-hoc constitutive models for the process zone (the region ahead of the crack tip where most of the dissipative events occur), which possibly includes rate and temperature dependence; ii) the definition of accurate numerical schemes for the simulation of fracture propagation, crack tip velocity fluctuation, and material fragmentation.

[*]Corresponding author, e-mail: stefano.mariani@polimi.it

In both cases, a fully macroscopic approach – where the microstructural features of the delamination are accounted for solely by using phenomenological models – could introduce a severe limit on the a" methods represent a promising tool, since they are specifically built to capture the details of all the time/space scales involved in the description of the problem.

In the simple cases of linear and nonlinear elasticity, wave propagation in heterogeneous materials has been simulated through asymptotic analysis (see, e.g., [7]). However, when dissipative processes are involved, as is the case with delamination in composites, analytical and numerical results are seldom available.

This paper reports on the simulation of the propagation of interlaminar debonding in composite laminates under dynamic loading by applying a coupled space-time multiscale scheme. The computational convenience of the multiscale method derives from the fine space/time scale resolution of the traction distribution in the process zone and the coarse resolution in the remaining domain. Annoying spurious problems often introduced by fine space discretization are the high frequency oscillations of the solution. The accuracy of the numerical solution was ensured by adopting a time integration algorithm (α-method [8]) able to damp spurious oscillation modes.

As the purpose was the presentation and assessment of the multiscale method performance, only tests concerning a single lamina which separates from a rigid substrate were considered. In particular, a two-stage peel test described in [1, 9, 10] was analysed: a thin lamina partially debonded from a substrate is statically deformed at fixed crack length; thus the constraints are relaxed and the stored elastic energy induces dynamic delamination growth. The results demonstrate that the proposed multiscale scheme accurately resolves the nonlinearities characterizing the process zone at a much reduced computational cost compared to full scale finite element simulations.

2. Problem formulation

Polymer matrix laminates used in standard delamination tests are assembled by bonding with resin-enriched interlayers a stacking sequence of laminae. Interlayers have small, although not totally negligible, thickness in comparison with one of the assembled laminate. Referring to a standard laminate used in the experiments, in the simulations a single pre-existing interlaminar crack (at the topmost level) is allowed to propagate, while the rest of the composite is assimilated to a rigid substrate. The mechanical properties of the separating interlayer are accordingly lumped to the zero-thickness surface Γ.

The problem at hand is described in Fig. 1. A thin layer is partially bonded to a rigid substrate through a cohesive surface Γ. The lamina small thickness allows to disregard shear deformations with respect to bending deflections. Thus, the motion of the thin layer under dynamic loadings in the small displacement regime is accurately modelled by the Euler–Bernoulli beam theory:

$$\rho A u_{,tt} + EI u_{,xxxx} + b\sigma(u) = 0 \tag{1}$$

where t is time, x is the lamina longitudinal axis coordinate; ρ is the material mass density, E the effective material's Young's modulus depending on the out-of-plane confinement of the displacement field, $A = bh$ and $I = bh^3/12$ the area and the moment of inertia of the lamina cross-section respectively, $u = u(x; t)$ the transversal displacement of the longitudinal axis, and the $\sigma(u)$ the normal cohesive traction between lamina and substrate.

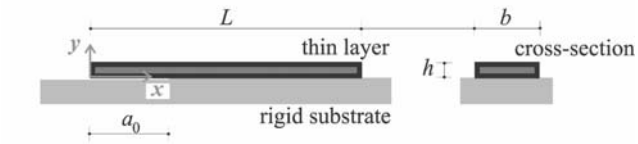

Fig. 1. Geometry of the lamina bonded to the rigid substrate

The loading conditions in a first stage are imposed by assigning the displacement history of the free end of the beam, $\bar{u}(t) = u(0; t)$. The imposed displacement $\bar{u}$ grows smoothly with time, to avoid the activation of higher order oscillation modes in the specimen. In this way, the adopted kinematics adequately describes the motion of the beam (see also [10]).

The test configuration is characterized by an initial crack of length a_0 (see Fig. 1). For $x \in [0; a_0)$ the vertical displacement must be positive on null, as a consequence of the impenetrability constraint given by the substrate. In the debonding region $x \in [a_0; L]$, the crack growth is modelled by a softening $\sigma = \sigma(u)$ relationship. According to classical cohesive theories in nonlinear fracture mechanics, a piecewise linear model is assumed (see Fig. 2):

$$\sigma(u) = \begin{cases} \sigma_M \dfrac{u/u_c}{\delta} & \text{if} \quad \leq \delta u_c \\ \sigma_M \dfrac{1-u/u_c}{1-\delta} & \text{if} \quad \delta u_c \leq u \leq u_c \\ 0 & \text{if} \quad u \geq u_c \end{cases} \tag{2}$$

where σ_M is the cohesive strength, u_c the critical opening displacement (beyond which the tensile response of the material vanishes), and δ a constitutive parameter defining the opening displacement at the stress peak. The parameter δ can be thought as an expedient to introduce an initial "elastic" stiffness.

The elastic branch of the cohesive law, for $u \leq \delta u_c$, is representative of the response of the interlayer prior to the localization of microscopic damage mechanisms, eventually leading to the formation of a well-defined macrocrack.

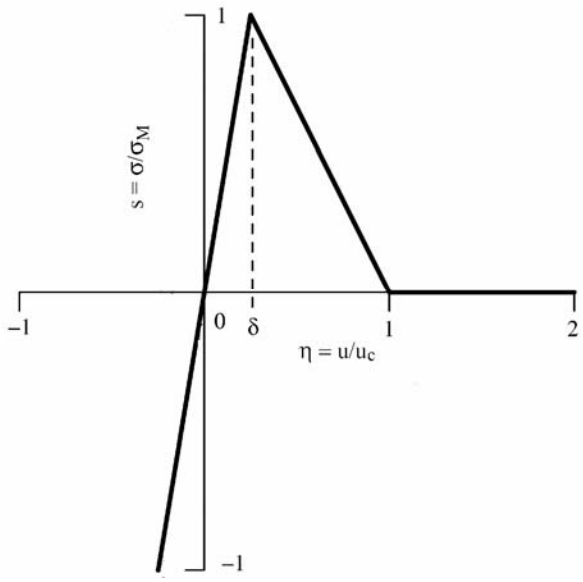

Fig. 2. Adopted piecewise linear cohesive law

The interface law (2) is path-independent or holonomic for $u < u_c$. Rate sensitive cohesive laws $\sigma(u; \dot{u})$, which explicitly include the dependence on the opening velocity, thus more suitable to describe rate-dependent experimental results in the low velocity crack growth regime [10] are not considered in this work.

As already pointed out [9, 4], cohesive models of fracture introduce characteristic length- and time scales into the material description.

The characteristic length l_c is defined as:

$$l_c = \frac{EG_c}{\sigma_M^2} \tag{3}$$

where $G_c = \int_0^\infty \sigma(u)du$ is the critical energy release rate, i. e. the energy spent for a unit increase of the extension of the crack surface Γ. The intrinsic length l_c roughly estimates the size of the process zone, where the crack opening takes place.

The characteristic (cohesive) time t_c is:

$$t_c = \frac{\rho c_L u_c}{2\sigma_M} \tag{4}$$

where c_L is the longitudinal wave speed, $c_L = \sqrt{E/\rho}$. The intrinsic time t_c arises from the interplay between material inertia and cohesive properties under dynamic conditions.

An additional time scale characterizes the problem in Fig. 1. The geometric time t_g is the time spent by a longitudinal wave to travel along the initially free part of the specimen, i.e.:

$$t_g = \frac{a_0}{c_L} \tag{5}$$

Equation (1) can be conveniently written in a more manageable form, pointing out the two time scales, by introducing the following non-dimensional time, space, displacement, and traction variables:

$$\tau = \frac{t}{t_g}, \qquad \xi = \frac{x}{a_0}, \qquad \eta = \frac{u}{u_c}, \qquad s = \frac{\sigma}{\sigma_M} \tag{6}$$

Thus the normalized equation of motion reads:

$$\eta_{,\tau\tau} + \frac{1}{12\lambda^2}\eta_{,\xi\xi\xi\xi} + \frac{1}{2}\frac{t_g}{t_c}\lambda s(\eta) = 0 \tag{7}$$

where $\lambda = a_0/h$ is the slenderness of the free part of the specimen at $t = 0$. Eq. (7) explicitly shows that the cohesive law $s(\eta)$ couples the two time scales t_c and t_g, which, in the case of standard composite materials, can differ by several orders of magnitude. This peculiarity must be accurately considered in devising numerical algorithms for the time integration of Eq. (7).

It should be emphasized that Eq. (7) additionally depends on two length scales. Besides the microstructural length scale l_c (Eq. (3)), measuring the extension of the active delamination zone, a macroscopic length scale, l_g, linked to the lengths a_0 and L can be introduced. In practice, the macroscopic scale l_g represents the actual size of the specimen, and, possibly, the scale of variation of the applied loading conditions. Depending on the material properties, the two space scales can also differ by several orders of magnitude.

3. Space-time multiscale approach

In spite of the simplicity of the problem at hand, the space-time multiscale nature of Eq. (7) is a challenging issue. In order to obtain an accurate numerical result one is compelled to use space and time discretization fine enough to capture the variation of the cohesive tractions within the smallest space and time scale. By making recourse to obvious uniformly fine space and time subdivisions, the analysis can quickly reach prohibitive computational costs. Additionally, the use of a fine discretization pushes the accumulation of numerical errors which inevitably spoil the quality of the solution.

As an alternative, a multiscale approach was used. Following the format typically employed by the heterogeneous multiscale method (HMM) for evolutionary problems [11], the method was cast into a two-step algorithm:

1. Force (residual) estimation:

a) reconstruction of the displacement field at the microscale;

b) solution of the governing equation at the microscale;

c) averaging the microscale solution into the macroscale variables.

2. Evolution of the displacement field at the macroscale.

The algorithm requires a double spatial discretization of Eq. (7). Two grids were introduced, with different spacing and location. The background, macroscopic grid is coarse and fixed, with node spacing $\Delta\xi_M$. The coarse grid covers the whole length of the specimen. The foreground, microscopic grid is much finer, with node spacing $\Delta\xi_m$, and moves with the crack tip. The fine discretization covers the region of Γ surrounding the process zone for an extension of 4–5 times the cohesive length scale l_c.

Adopting a classical finite difference scheme, the spatial derivative $\eta_{,\xi\xi\xi\xi}$ of the transversal displacement at the i-th node is second-order approximated as:

$$\eta^i_{,\xi\xi\xi\xi} = \frac{\eta^{i-2} - 4\eta^{i-1} + 6\eta^i - 4\eta^{i+1} + \eta^{i+2}}{\Delta\xi^4} \tag{8}$$

where $\Delta\xi$ takes the value $\Delta\xi_M$ or $\Delta\xi_m$, depending on the active grid. To link together the two approximations, continuity on displacement and rotations at the boundaries of the microscopic grid was imposed. This excludes the presence of kinks in the discrete solution.

The semi-discrete form of the original partial differential equation is given by the following system of ordinary differential equations:

$$\begin{aligned} &\eta^I_{,\tau\tau} + \frac{1}{12\lambda^2}\frac{\eta^{I-2} - 4\eta^{I-1} + 6\eta^I - 4\eta^{I+1} + \eta^{I+2}}{\Delta\xi_M^4} + \frac{1}{2}\frac{t_g}{t_c}\lambda s(\eta^I) = 0, \quad I = 1, ..., I_M \\ &\eta^i_{,\tau\tau} + \frac{1}{12\lambda^2}\frac{\eta^{i-2} - 4\eta^i + 6\eta^i - 4\eta^{i+1} + \eta^{i+2}}{\Delta\xi_m^4} + \frac{1}{2}\frac{t_g}{t_c}\lambda s(\eta^i) = 0, \quad i = 1, ..., I_m \end{aligned} \tag{9}$$

where I_M and I_m are the number of nodes in the macroscopic and microscopic grids, respectively.

The initial conditions for Eq. (9) are:

$$\begin{aligned} &\eta^I(\tau = 0) = \eta^{I(0)} \qquad \eta^i_{,\tau}(\tau = 0) = \eta^{I(0)}_{,\tau}, \quad I = 1, ..., I_M \\ &\eta^i(\tau = 0) = \eta^{i(0)} \qquad \eta^i_{,\tau}(\tau = 0) = \eta^{i(0)}_{,\tau}, \quad i = 1, ..., I_m \end{aligned} \tag{10}$$

It is well known [12] that the Euler–Bernoulli equation is dispersive, i.e., every frequency of the solution propagates with its own velocity. The fine space grid allows the local capture of high frequency oscillations, characterized by increasing propagation speeds as the node spacing $\Delta\xi_m$ reduces.

The initial value problem (9)–(10) is thus integrated in time with the explicit α-method [8]. The α-method possesses the positive feature to numerically filter out of the solution high frequency oscillations, thus conserving the order of accuracy of the scheme.

The multiscale solution in the time step $[\tau^{(n)}, \tau^{(n+1)}]$, with $\tau^{(n+1)} = \tau^{(n)} + \Delta\tau_M$, is described in Table 1. The constants α, β, and γ are algorithmic coefficients.

Table 1. Explicit time integration algorithm

(1) Microscopic fields $(i = 1, ..., I_m)$, for $k = 0, K-1$:

- predictor phase:

$$\bar{\eta}^{i(n+1,k+1)} = \eta^{i(n+1,k)} + \Delta\tau_m \eta^{i(n+1,k)}_{,\tau} + \frac{\Delta\tau_m^2}{2}(1-2\beta)\eta^{i(n+1,k)}_{,\tau\tau}$$

$$\bar{\eta}^{i(n+1,k+1)}_{,\tau} = \eta^{i(n+1,k)}_{,\tau} + \Delta\tau_m(1-\gamma)\eta^{i(n+1,k)}_{,\tau\tau}$$

- solution phase:

$$\eta^{i(n+1,k+1)}_{,\tau\tau} = -\frac{1}{12\lambda^2}\frac{\tilde{\eta}^{i-2} - 4\tilde{\eta}^{i-1} + 6\tilde{\eta}^{i} - 4\tilde{\eta}^{i+1} + \tilde{\eta}^{i+2}}{\Delta\xi_m^4} - \frac{1}{2}\frac{t_g}{t_c}\lambda\, s(\tilde{\eta}^i)$$

where:

$$\tilde{\eta}^i = (1+\alpha)\bar{\eta}^{i(n+1,k+1)} - \alpha\,\eta^{i(n+1,k)}$$

- corrector phase:

$$\eta^{i(n+1,k+1)} = \bar{\eta}^{i(n+1,k+1)} + \Delta\tau_m^2\beta\,\eta^{i(n+1,k+1)}_{,\tau\tau}$$

$$\eta^{i(n+1,k+1)}_{,\tau} = \bar{\eta}^{i(n+1,k+1)}_{,\tau} + \Delta\tau_m\gamma\,\eta^{i(n+1,k+1)}_{,\tau\tau}$$

(2) Macroscopic fields $(I = 1, ..., I_M)$:

- predictor phase:

$$\bar{\eta}^{I(n+1)} = \eta^{I(n)} + \Delta\tau_M \eta^{I(n)}_{,\tau} + \frac{\Delta\tau_M^2}{2}(1-2\beta)\eta^{I(n)}_{,\tau\tau}$$

$$\bar{\eta}^{I(n+1)}_{,\tau} = \eta^{I(n)}_{,\tau} + \Delta\tau_M(1-\gamma)\eta^{I(n)}_{,\tau\tau}$$

- solution phase:

$$\eta^{I(n+1)}_{,\tau\tau} = -\frac{1}{12\lambda^2}\frac{\tilde{\eta}^{I-2} - 4\tilde{\eta}^{I-1} + 6\tilde{\eta}^{I} - 4\tilde{\eta}^{I+1} + \tilde{\eta}^{I+2}}{\Delta\xi_M^4} - \frac{1}{2}\frac{t_g}{t_c}\lambda\, s(\tilde{\eta}^I)$$

where:

$$\tilde{\eta}^I = (1+\alpha)\bar{\eta}^{I(n+1)} - \alpha\,\eta^{I(n)}$$

- corrector phase:

$$\eta^{I(n+1)} = \bar{\eta}^{I(n+1)} + \Delta\tau_M^2\beta\,\eta^{I(n+1)}_{,\tau\tau}$$

$$\eta^{I(n+1)}_{,\tau} = \bar{\eta}^{I(n+1)}_{,\tau} + \Delta\tau_M\gamma\,\eta^{I(n+1)}_{,\tau\tau}$$

It is assumed that at the beginning of the time step the solution is completely known in terms of the displacement, velocity and acceleration fields. The time steps $\Delta\tau_M$ and $\Delta\tau_m = \Delta\tau_M/K$ are chosen to satisfy the Courant, Friedrichs and Lewy numerical stability conditions for the propagation of stress waves in solids. In particular, to ensure that in the solution the waves do not propagate faster than the actual longitudinal wave speed

$$\Delta\tau_M = \frac{1}{\vartheta}\frac{\Delta\xi_M}{\gamma_L}, \qquad \Delta\tau_m = \frac{1}{\vartheta}\frac{\Delta\xi_m}{\gamma_L} \tag{11}$$

were set, where $\gamma_L = t_g c_L/a_0$ is the normalized speed of longitudinal waves, ϑ a reducing factor, typically assumed $\vartheta = 10$–20. The integer ratio K is kept constant along the whole analysis. According to Table 1, the HMM scheme repeats the step (1) K times in order to cover a single macroscopic step $\Delta\tau_M$. The macroscopic solution can be advanced in time only when the sequence of K microscopic steps is accomplished.

4. Numerical results

The two-stage test described in section 1 has been previously analyzed with finite elements in [9]. The results of those calculations pointed out that during the initial, transient phase of the second stage transversal waves emitted from the crack tip are reflected on the top surface of the layer, affecting the crack growth speed. Once the transient phase is completed, the lamina behaves as a beam, and its response is mainly governed by longitudinally propagating waves.

The macroscopic boundary conditions imposed in the second phase of the analysis are:

$$\begin{aligned} &\eta = \bar{\eta}, \quad \eta_{,\xi\xi} = 0 \quad \text{at} \quad \xi = 0, \forall\tau \\ &\eta_{,\xi\xi} = \eta_{,\xi\xi\xi} = 0 \quad \text{at} \quad \xi = \frac{L}{a_0}, \forall\tau \end{aligned} \tag{12}$$

i.e., at the left end, the transversal displacement is held fixed, the rotation is free, and the bending moment is null; at the right end, both displacement and rotation are free, while shear and bending moment are null.

The material of the lamina is alumina, characterized by the density $\rho = 3690$ kg/m^3, Young's modulus $E = 260$ GPa, cohesive strength $\sigma_M = 400$ MPa, critical energy release rate $G_c = 34$ J/m^2, and longitudinal wave speed $c_L = 8394$ m/s. In the calculation $\delta = 0.01$ was assumed. A higher value of δ could allow better matching to the finite element simulation results [9], but it would also spoil the solution by introducing severe numerical instabilities.

The dimensions of the specimen are $a_0 = 0.4$ mm, $L = 12$ mm, and $h = 0.2$ mm (b assumed unitary). The ratio L/a_0 is high enough to exclude, in the time interval of interest, wave reflection effects on the crack propagation.

The values of the characteristic times and lengths thus are t_c = 0.0066 μs, t_g = 0.0477 μs, l_c = 55.25 μm, and l_g = 400 μm. The nodal spacings adopted in the simulations are Δx_M = 50 μm for the background grid, and $\Delta x_M \leq 11.05$ μm (at least 5 elements to cover l_c) for the process zone.

Figure 3 shows the crack tip history for two different values of the initially imposed displacement $\bar{u}$.

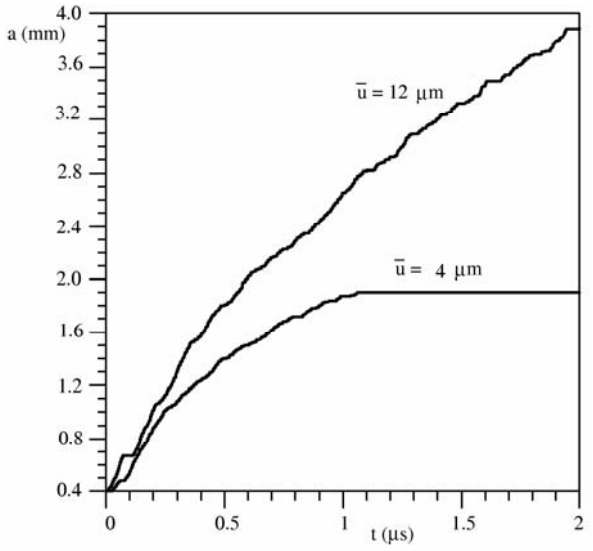

Fig. 3. Peel test: effect of the imposed displacement $\bar{u}$ on crack growth

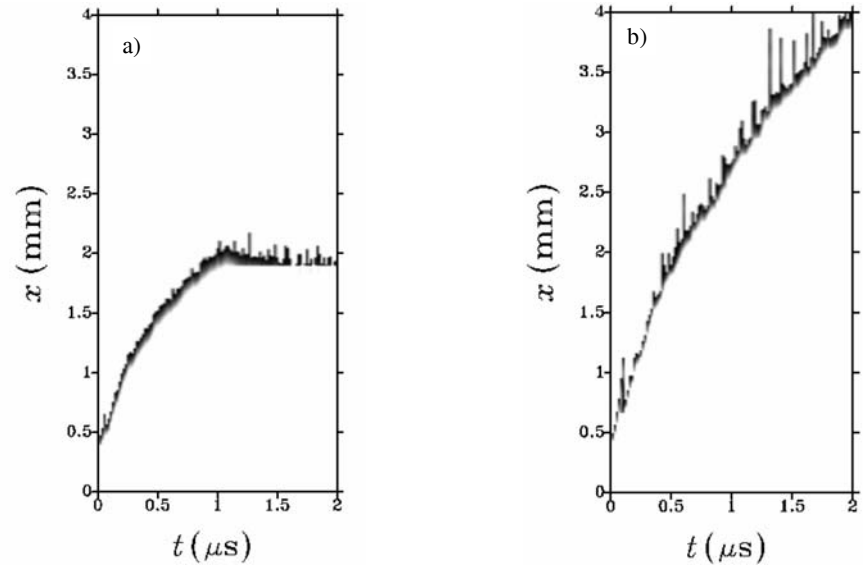

Fig. 4. Peel test: space-time map of the active process zone: a) $\bar{u}$ = 4 μm, b) $\bar{u}$ = 12 μm

Assigning a small initial displacement as $\bar{u} = 4$ μm, the specimen stores a small amount of elastic energy, sufficient to start the dynamic delamination, but not to complete the separation process. In fact, after about 1 μs the crack speed drastically reduces and finally the crack arrests at $a_f = 1.9$ mm. For a bigger initial displacement, as $\bar{u} = 12$ μm, the stored elastic energy is big enough to start and maintain crack growth, although the crack speed monotonically reduces with time.

Figure 4 shows (for the small and large initial displacements), space-time maps of the active process zone location. The dark regions in the plots indicate the region (ahead of the current crack tip), where $u \geq u_c$ and $u_{,t} > 0$. Sudden variations of the process zone length are a consequence of the interaction between the transversal waves released from the crack tip and the layer deformation due to the elastic branch of the cohesive law. Such variation should disappear for high elastic slopes, i.e. for $\delta \to 0$. It is interesting to observe that, for a given imposed displacement, the extension of the active process zone is generally constant, independent of the effective crack speed, except for the mentioned peaks.

5. Concluding remarks

A simple space-time coupled multiscale approach for the solution of an interesting and difficult problem in composite fracture mechanics, i.e. the delamination under dynamic loading, has been presented. The approach is based on a double discretization of the model, with a coarse grid in the structure and a fine grid, moving with the crack tip location, surrounding the process zone. Time discretization follows the space grids, in order to satisfy Courant's stability requirement. Overall the method is second order accurate. The advantages of such a multiscale method could be exploited for more complicated problems, as in the case of rate-dependent or temperature-dependent materials, where more than two time scales are involved. In future works, concerning rate-dependent material models, it is intended to apply the proposed multiscale methodology to a finite element discretization of the continuum.

Acknowledgements

S.M. and A.P. gratefully acknowledge the financial support provided by MIUR through the Cofin 2003 programme *Interfacial damage failure in structural systems: applications to civil engineering and emerging research fields*.

References

[1] FREUND L.B., *Dynamic Fracture Mechanics*, Cambridge University Press, 1990.
[2] XU X.-P., NEEDLEMAN A., J. Mech. Phys. Solids, 42 (1994) 1397.
[3] YANG B., RAVI -CHANDAR K., J. Mech. Phys. Solids, 44 (1996), 1955.
[4] PANDOLFI A., KRYSL P., ORTIZ M., Int. J. Fracture, 95 (1999), 1.
[5] ROSAKIS A.J., Adv. Phys., 51 (2002),1189.
[6] COSTANZO F., WALTON J.R., J. Mech. Phys. Solids, 50 (2002),1649.

[7] YU Q., FISH J., Int. J. Solids Struct., 39 (2002), 6429.
[8] HILBER H.M., HUGHES T.J.R., TAYLOR R.L., Earthquake Eng. Struct. Dynamics, 5 (1977), 283.
[9] CAMACHO G.T., ORTIZ M., Int. J. Solids Struct., 33 (1996), 2899.
[10] CORIGLIANO A., MARIANI S., PANDOLFI A., Compos. Sci.e Technol., to appear, 2005.
[11] E W., ENGQUIST B., Commun. Math. Sciences, 1 (2003), 87.
[12] STRIKWERDA J.C., *Finite Difference Schemes and Partial Differential Equations*, Chapman & Hall, 1989.

Received 6 September 2004
Revised 4 January 2005